Unmanned Systems, Vol. 2, No. 2 (2014) 121–141

DOI: 10.1142/S2301385014500083

UNMANNED SYSTEMS
http://www.worldscientific.com/worldscinet/us

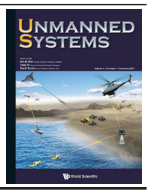

Systematic Design and Implementation of a Micro Unmanned Quadrotor System

Swee King Phang[*,§], Kun Li[†], Kok Hwa Yu[‡], Ben M. Chen[†], Tong Heng Lee[†]

[*]*NUS Graduate School for Integrative Sciences and Engineering, National University of Singapore, 21 Lower Kent Ridge Road, Singapore 119077*

[†]*Electrical and Computer Engineering, National University of Singapore, 21 Lower Kent Ridge Road, Singapore 119077*

[‡]*Mechanical Engineering, National University of Singapore, 21 Lower Kent Ridge Road, Singapore 119077*

This paper presents a guideline to systematically design and construct a micro quadrotor unmanned aerial vehicle (UAV), capable of autonomous flight. The designed micro UAV has a gross weight of less than 40 g including power supply sufficient for an 8-min flight. The design is divided into three parts. First, investigation is made on the structural design of a conventional quadrotor. The quadrotor frame is then carefully designed to avoid any potential structural natural frequencies within the range of rotors operating speeds, based on simulation results obtained from MSC Nastran. Second, avionic system of the aircraft will be discussed in detail, mainly focusing on the design of printed circuit boards which include sensors, microprocessors and four electronic speed controllers, specially catered for micro quadrotor design. Last, a mathematical model for the micro quadrotor is derived based on Newton–Euler formalism, followed by methods of identifying the parameters. The flight test results are later described, analyzed and illustrated in this paper.

Keywords: Finite elemental analysis; nonlinear model; UAV control; structural analysis.

US

Nomenclature

$\mathbf{P_n}$: Position vector in North-East-Down frame
$\mathbf{V_b}$: Velocity vector in body frame
$\mathbf{\Theta}$: Euler angles
ω : Angular velocity vector
δ_n : Normalized input to the nth motor
g : Gravitational acceleration
J : Moment of inertia of aircraft's body
J_r : Moment of inertia of a rotating propeller
k_T : Thrust constant
k_Q : Moment constant
l : Length of a single quadrotor's arm
m : Mass of the aircraft
Ω_n : nth propeller rotational speed
Q_n : Torque produced by the nth propeller
T_n : Thrust produced by the nth propeller

Received 14 October 2013; Revised 19 December 2013; Accepted 3 January 2014; Published 5 March 2014. This paper was recommended for publication in its revised form by editorial board member, Guowei Cai.
Email Address: §*king@nus.edu.sg*

1. Introduction

Unmanned aerial vehicles (UAVs) are currently playing major roles not only in military tasks but also in civilian applications. Their mobile capability, which is an advantage over the ground vehicles, makes them the ideal platform for tasks such as exploration, environment monitoring, search and rescue, and security surveillance missions [32]. They are also used for delivery of payloads in complex indoor or outdoor environments. To date, researchers around the globe have developed many UAV platforms in various sizes to realize these tasks. Besides the conventional fixed-wings [14] and rotorcrafts [17,19], many new platforms such as flapping wings and ducted fans aircraft are introduced

[2,11,13,18,24,26,31]. Some researchers are also motivated to design unconventional hybrid aircrafts, such as vertical takeoff and landing (VTOL) fixed-wings UAV to realize navigation in cluttered environments [9,16,23].

In recent years, extensive researches have been directed to the development of micro-aerial vehicles (MAVs), which are the miniature size of UAVs. Since 1997, the Defense Advanced Research Projects Agency (DARPA) has initiated a program to develop and test MAVs for military surveillance and reconnaissance missions. In DARPA's definition, an MAV needs to fulfill the following three criteria [30]:

(1) Maximum dimension of the aircraft in any direction to be no longer than 15 cm (6 inches);
(2) Gross weight should not be exceeding 100 g, with up to 20 g devoted to payload;
(3) The aircraft should be able to reach an altitude of 100 m.

One can easily see that the limited dimension and weight budget pose a big problem in the onboard components choices, such as inertial measurement unit (IMU) which is essential for aircraft control and navigation, and the camera for visual monitoring purposes. Today, fortunately, with smarter electronic sensors, processors, and actuators realized in smaller and lighter packages, the implementation of such MAV is made possible. In order to realize even lighter UAV or MAV, it is, however, not sufficiently good enough if we utilize commercial products for each onboard component. Researchers from some institutions have started to develop part of their onboard system from circuit level [1]. For example, PixHawk UAV from ETH is embedded with a self-customized processor board for their onboard vision processing [20]. Research partners such as Ascending Technologies also offer customization of UAV based on requests from partner universities [21]. To fulfill the size and weight limitation on the MAV, circuit design is unavoidable. In this paper, we proposed a design of a full onboard system down to the circuit level. It includes processors, IMU and motor electronic speed controllers (ESCs), on a single piece of printed circuit board (PCB). With this proposal, the whole avionic system can be constrained within 8 g. A fully functional MAV built in accordance to this guideline is shown in Fig. 1.

Another main issue arising in miniature aircrafts is the structural vibration issue. It is, however, commonly ignored or avoided by utilizing stiffer material if a large payload budget is permitted. Bounded by the design requirements mentioned above, the MAV is constructed at the expense of structural stability. At small scale, the device is structurally fragile and thus it is more vulnerable to variety of potential structural vibration problems especially the structural resonance. In this condition, the vibration is amplified to a maximum amplitude when the forcing frequency matches

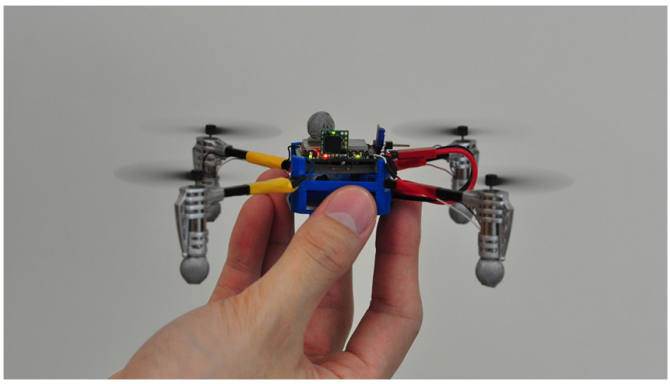

Fig. 1. A working model of the proposed MAV design.

the natural frequency of the structure [10]. For example, in MAVs of quadrotor platforms, slender bodies such as the arms are typically susceptible to this harmful threat. When structural vibration is present, it may lead to degraded sensor performance and even mechanical damage if it is allowed for a period of time [25]. This is more likely to occur as quadrotor frame is commonly made of composite materials which are much lighter. Therefore, the quadrotor frame needs to be carefully designed to avoid any potential structural natural frequencies within the range of its rotors operating speed.

This paper is divided as follows: In Sec. 2, we are focusing on solving the structural vibration problem related to micro quadrotor UAV design. Structural analysis is performed on the proposed micro quadrotor platform, which includes several different arm shape designs. With the results obtained above, Sec. 3 details the design of the bare quadrotor hardware, including the frame design and motor selection. The implementation of the avionic system which includes most of the onboard components will be discussed in Sec. 4. Section 5 shows the derivation of a nonlinear mathematical model of the proposed micro quadrotor, based on Newton–Euler formalism. Lastly, Sec. 6 presents the model verification results and autonomous flight control results carried out in a room equipped with Vicon motion tracking system. Overall concluding remarks will be made in the last section.

2. Finite Element Analysis of Platform Structure

The design of a realistic MAV requires a rigorous analysis and testing process [7]. First, a stable MAV platform is necessary to achieve efficiency and reliability in MAV operation. Before we analyze the structural behavior of MAV, it is important to examine the source of vibration in

the aircraft design. Several important sources of vibration on helicopter are identified by Cai *et al.* [6] and Ceruti *et al.* [8]. Elsewhere, a comprehensive vibration analysis of the UAV helicopter is pursued by Plasencia *et al.* [28]. In the MAV environment, the structural components may vibrate due to mechanical and aerodynamic effects. Looking at the configuration of a quadrotor, the major contribution towards the vibration issue is attributed to the engine powered rotating rotors. Mounted on the tip of the quadrotor arms, these rotors create a periodic excitation which caused vibration. To conduct fast and reliable structure analysis, finite element analysis (FEA) via MSC Nastran is used in the present work. Using this approach, it offers great flexibility to model complex geometries which would be impossible by taking analytical approach. Discretized into finite number of elements, the stresses and displacements of parts and assemblies under internal and external loads can be calculated. In additional, natural mode analysis is conducted to determine the natural frequencies and mode shapes of the model. This leads to the prediction of resonance for the structure and the type of resonance that may occur during the MAV flight operation. On the other hand, frequency response analysis is used to determine the displacement response of the model when external steady-state oscillatory excitation (simulating rotor rotation) is applied.

2.1. *Vibration frequency analysis*

Although the main source of vibration has been identified, it is still a challenging task to investigate the complex interactions between structural, inertial and aerodynamic forces acting on the MAV structure. Therefore, structural analysis is pursued to analyze the structural stiffness in avoiding the resonant problem. As mentioned above, the flexible characteristics of the MAV components, especially the quadrotor arms are frequently exposed to undesired vibrations. In the design, in order to perform basic maneuvering, the micro quadrotor is required to have up to 60 g thrust as it is approximately 1.5 times its own weight. As each rotor is subjected to a uniform load, each propeller is expected to provide at least 15 g of thrust. Here, the relative gearbox vibration is neglected as the propeller is directly driven by the motor. Using the estimated rotor load, the operating range of the rotor is determined experimentally. Based on the propeller chosen in this design, rotational speed below 330 revolutions per second is found to be sufficient to provide the required thrust to perform the task. In other words, the 1st mode natural frequency of the aircraft structure must be much larger than 330 Hz to avoid resonance.

In the following subsections, natural modes of a few different frame designs for small scale quadrotor will be studied systematically by utilizing the commercial software MSC Nastran. A few possible material were simulated, such as plastic, aluminum and carbon fiber. Note that only the results from the carbon fiber simulation are shown in this paper as it exhibits the best stiffness against weight ratio among the chosen materials.

2.2. *Single quadrotor arm*

Conventionally, a quadrotor UAV consists of four extended arms attached to a square body which holds the onboard system including sensors, processors and receiver. As the load is shared uniformly on each rotor, the structural analysis on single quadrotor arm can provide a good insight before we analyze the full quadrotor configuration. There are many factors that influence the stiffness of the quadrotor arm, i.e., material, geometric parameter and shape. Under the constraint of weight and size, it is best to analyze a few different types of beam structure.

In this analysis, five types of different cantilever beam are designed and analyzed. The cross sections for each of the beams are shown in Fig. 2. In the simulation, a single quadrotor arm is treated as a cantilever beam which has a fixed end and a free end. A few different parameters on the dimension of the beams will be varied, and the corresponding natural mode (1 to 4) will be compared. Note that the composite material for all beams to be simulated has the properties of carbon fiber codename carbon/epoxy T300/976 as shown in Table 1.

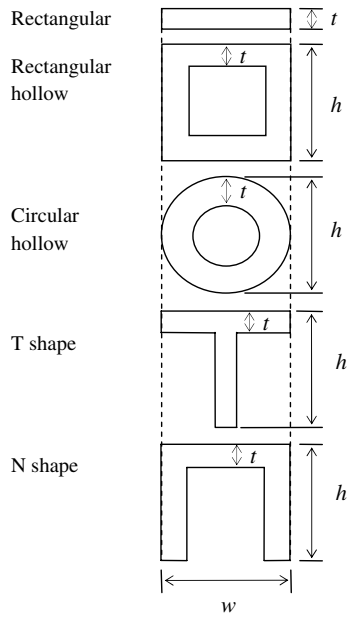

Fig. 2. Cross sections of five common beams.

Table 1. Properties of carbon/epoxy T300/976.

Property	Value
Modulus of elasticity (longitudinal direction)	135 GPa
Modulus of elasticity (transverse direction)	9.24 GPa
Poisson's ratio	0.32
Density	1480 kg/m^3

2.2.1. *Length of arm*

It is well known that slender bodies are more easily exposed to vibration, or in other words, shorter beams are stiffer. To verify the relationship between the length of the beam and its natural mode, rectangular beams (first cross section in Fig. 2) with different lengths are analyzed in the simulation. For this analysis, the discrete element employed has six degrees of freedom per node and all nodes at one of the tip are assumed to be fixed by setting all six degrees of freedom to zero. In Table 2, a summary of the Nastran natural mode analysis results obtained for this study is given.

Based on the simulation results, it is evident that natural frequencies for all first four modes increased when the structure is shorter. In general, beams of other shapes show similar behavior and thus the results are trivial and not to be included in this paper. Intuitively, the quadrotor arms are structurally more stable and resonance at low frequencies can be avoided if it is shorter. Given the restriction on the minimum length between rotor and mass center, an optimum length of quadrotor arm is desired. This is to ensure the aerodynamic interferences between the rotors could be minimized. Therefore, a minimum length of the quadrotor arms is prescribed to be twice of the rotor radius.

2.2.2. *Thickness of beam*

Two common thicknesses of commercially available carbon fiber sheets or beams are 0.5 and 1 mm. Since the primary concern in building an MAV quadrotor is the weight limit, the natural mode of all five general shapes of beams are analyzed and compared. Here, the model for each cross section was constructed with length $l = 60$ mm, width $w = 6$ mm and height $h = 6$ mm (see Fig. 2 for illustration). Following the similar procedure for the normal mode analysis, only the first two natural modes for each model are tabulated. Table 3 shows the results for beam with thickness $t = 1$ mm, while Table 4 shows the results for beam with thickness $t = 0.5$ mm, together with their calculated weight.

As one can observe from Fig. 3, the first and second mode shapes for rectangular beam are associated with vertical bending. In this condition, the vibration amplitude is maximized at the tip of the arm. Moreover, the natural frequencies for rectangular beam structure simulated are relatively low, thereby prohibiting the usability of the rectangular beam. As we examine Tables 3 and 4, beams with closed shape configurations (rectangular hollow and circular hollow) yield the highest natural frequencies amongst all, well within the maximum operating requirement. Comparing the results between 0.5 mm thickness beams to their counterpart of 1 mm thickness, the natural frequencies are not significantly affected although the weight is half of the latter one. This is validated experimentally, provided the thickness is not sufficiently thin.

In addition, although the N-shape and T-shape configurations give better weight budgets, their natural frequencies are comparatively much lower than that of rectangular hollow and circular hollow shapes, which are in the closed cross section forms.

Table 2. Natural frequencies of thin plate.

	Natural frequency (Hz)			
Length (mm)	Mode 1	Mode 2	Mode 3	Mode 4
50	614.6	3656.7	3803.4	10518
60	426.85	2546.1	2642.6	7313.4
70	313.62	1873.6	1942.1	5377.1
80	240.3	1437.1	1491.3	4137.1
90	189.73	1135.4	1175.3	3255.4
100	153.68	920.14	952.05	2637.5

Table 3. Natural frequencies of beams of 1 mm thickness.

		Natural frequency (Hz)	
Type of cross section	Weight (g)	Mode 1	Mode 2
Rectangular	0.5328	426.85	2546.1
Rectangular hollow	1.776	3032.4	17,318
Circular hollow	1.3949	2647.9	15,624
T shape	0.9768	1902.8	2622.7
N shape	1.4208	2717.5	3215.6

Table 4. Natural frequencies of beams of 0.5 mm thickness.

		Natural frequency (Hz)	
Type of cross section	Weight (g)	Mode 1	Mode 2
Rectangular	0.2664	213.45	1322.5
Rectangular hollow	0.9768	3270.7	18,312
Circular hollow	0.767	2851.6	16,495
T shape	0.5106	1845.3	2713.2
N shape	0.7548	2810.4	3458.7

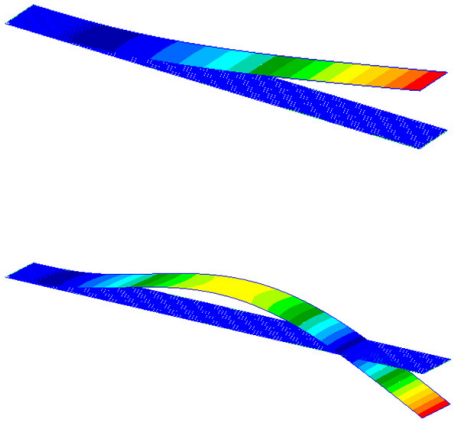

Fig. 3. Mode shape for rectangular shaped beam.

Table 6. Circular hollow beam with 0.5 mm thickness.

Radius (mm)	Natural frequency (Hz)			
	Mode 1	Mode 2	Mode 3	Mode 4
2.0	1839.3	1839.3	11,070	11,070
2.5	2347.5	2347.5	13,875	13,875
3.0	2851.6	2851.6	16,495	16,495
3.5	3349.6	3349.6	18,911	18,911
4.0	3840.1	3840.1	21,117	21,117
4.5	4322.0	4322.0	23,116	23,116
5.0	4794.3	4794.3	24,918	24,918
5.5	5256.1	5256.1	26,538	26,538

2.2.3. *Width and height*

Based on the results obtained in Sec. 2.2.2, the investigation is now focused on the closed shape beam. In this section, the effects of width and height of rectangular hollow beam and radius of circular hollow beam are investigated.

For rectangular hollow beam, the first and second modes are associated with the horizontal and vertical bending. It can be seen from Table 5 that the height variation of the rectangular hollow beam affects the horizontal bending mode more severely than the vertical one. On the other hand, the effect of width variation of the beam is vice versa. When a square beam with equal height and width is used, it will give similar frequencies for 1st and 2nd mode. This is further proven in Table 6 where the circular hollow beams were analyzed.

2.3. *Full quadrotor configuration*

Due to structure stability shown by closed shape beams, the full configuration is then tested using rectangular hollow beam and circular hollow beam to form the arms attached to each corner of the main frame. The main frame is designed to be 28.28 × 28.28 mm with thickness 2 mm. For simulation purpose, the main frame is made of aluminum with modulus of elasticity 70 GPa and Poissons ratio 0.3 with density 2700 kg/m^3. Meanwhile, 60 mm long beam is employed as the quadrotor arm. Again, unidirectional carbon/epoxy T300/976 is used. The main frame is modeled as 2D shell element while the quadrotor arm using 1D beam, as shown in Fig. 4.

For this analysis, the main frame is assumed to be rigid and thus, fixed in all three translation degrees of freedom. For a quadrotor model with 3 mm width, 3 mm height and 1 mm thickness rectangular hollow beam, the resulted natural frequencies for 1st and 2nd mode are 971.92 and 5843.3 Hz. On the other hand, the natural frequencies for quadrotor model using circular hollow beam with outer diameter of 3 mm and thickness of 1 mm are at 940.35 Hz for first mode and 5070.7 Hz for second mode.

Subsequently, dynamic analysis is performed to investigate the response of the quadrotor to oscillatory excitation produced by the propeller blades. To simulate 50 g of thrust from the propellers, 0.1225 N force is applied on each arm of the quadrotor. The analysis is performed over frequency

Table 5. Rectangular hollow beam with 0.5 mm thickness.

Height (mm)	Width (mm)	Natural frequency (Hz)			
		Mode 1	Mode 2	Mode 3	Mode 4
3	5	1625.9	2515.8	9673.4	14,904
3	6	1651.8	2979.7	9718.5	17,415
3	7	1670.3	3430.8	9708.0	19,762
3	8	1683.5	3871.3	9656.9	21,954
3	9	1693.0	4302.7	9576.0	23,571
3	10	1699.4	4725.6	9472.4	22,983
4	6	2218.0	3105.6	12,845	17,908
5	6	2756.0	3199.4	15,699	18,185
6	6	3270.7	3270.7	18,312	18,312

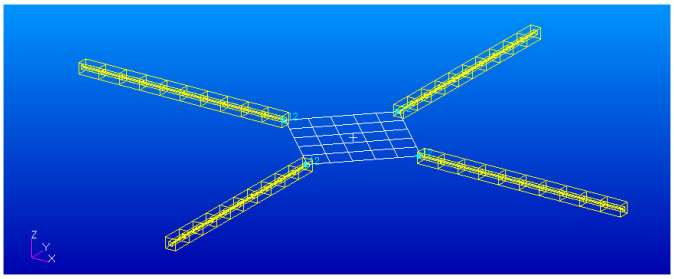

Fig. 4. Quadrotor model with rectangular hollow beams.

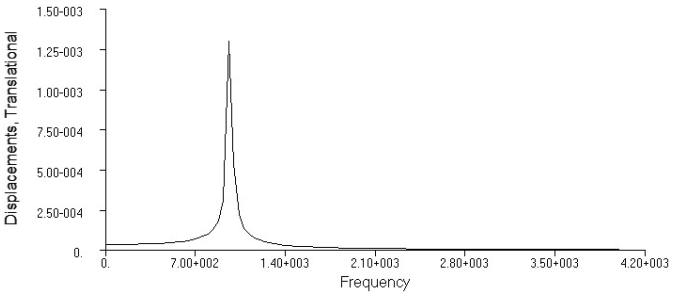

Fig. 5. Displacement response at tip of the arm of quadrotor model with rectangular hollow beam.

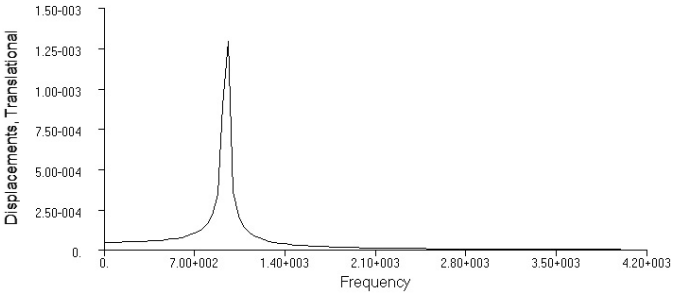

Fig. 6. Displacement response at tip of the arm of quadrotor model with circular hollow beam.

range of 0 to 4000 Hz. Results obtained from the Nastran are displayed in Figs. 5 and 6.

The results show the displacement amplitude at the tip of the quadrotor arm. From the response spectrum, the frequency at peak for both quadrotor models matched the first natural mode simulated earlier. Based on the simulation result, both models are suitable for miniature quadrotor design as the working frequency (330 Hz) is far from the natural frequency (971.92 Hz for quadrotor with rectangular hollow beam and 940.35 Hz for quadrotor with circular hollow beam) of the first mode. Therefore, using closed shape beam as the quadrotor arm can guarantee extreme stability for the whole quadrotor model.

3. Quadrotor Body Design

The previous section has illustrated the structural analysis for several beam candidates. It is noted that closed shape beams yield higher natural frequencies, thus outperforming the others. Oscillatory steady-state excitation representing the force induced by propeller is experimentally determined along with its working frequency. The external force is then applied on the tip of each quadrotor arm for frequency response analysis. The results show quadrotor models with either rectangular hollow or circular hollow cross section give significantly low displacement amplitude. Also, the natural frequency for both model are above 940 Hz which is far away from the working frequency of the proposed micro quadrotor. Therefore, rectangular hollow or circular hollow beams are the most suitable structures to form the quadrotor arms. In fact, they are widely available.

In this section, the quadrotor basic body design is proposed. It includes the following parts:

(1) A plastic body which holds the avionic system, power supply, and four extended arms;
(2) Four plastic holders for motors; and
(3) Four sets of suitable motor and propeller which provide sufficient lifting thrust for the quadrotor.

The following subsections detail the design of the mentioned frame and the selection of the motor and propeller.

3.1. *Quadrotor frame*

According to the results from the beam analysis, four carbon fiber tubes with the dimension of $60 \times 3 \times 3$ mm are utilized to connect four motors to the base frame. The base frame is designed with the aid of a 3D mechanical design software named SolidWorks. SolidWorks develops efficient and quicker designs of mechanical products and components, facilitating the design tasks for the platform. This 3D software is chosen as the design and analyzing software over other mechanical design tools for the following advantages:

(1) In-built intelligence design tools increase design efficiency and minimize design error;
(2) Better visualization of the design with intuitive interaction with the 3D model;
(3) Easy one click creation of 2D drawing from 3D objects for fabricating and manufacturing;
(4) Weights, center of gravity (CG), moment of inertia and other geometric data can be obtained directly from the evaluation functions; and
(5) Vibration and resonant frequencies simulation can be conducted with aid of SolidWorks simulation software.

The base frame is designed such that it holds four carbon fiber tubes, forming a symbolical cross shape of the quadrotor. Two partitions were created to mount the avionic PCB and to hold the battery. It can be visualized in Fig. 7.

Four light weight holders are designed to mount the electric motor at the end of each beam (see Fig. 8). Together with the base frame, they are fabricated with acrylonitrile butadiene styrene (ABS). The complete frame design for the micro quadrotor UAV can be visualized in Fig. 9.

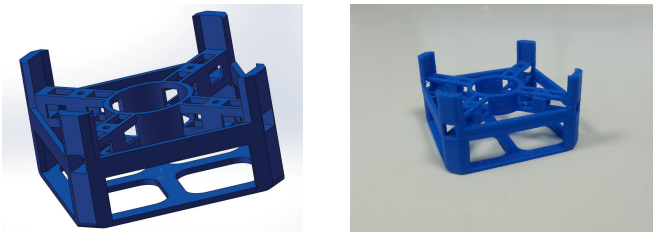

Fig. 7. Fabricated quadrotor body and its counterpart designed in SolidWorks.

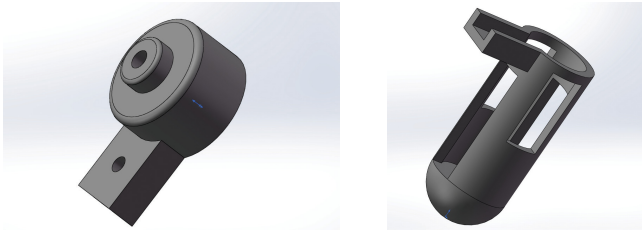

Fig. 8. Motor holder designed in SolidWorks.

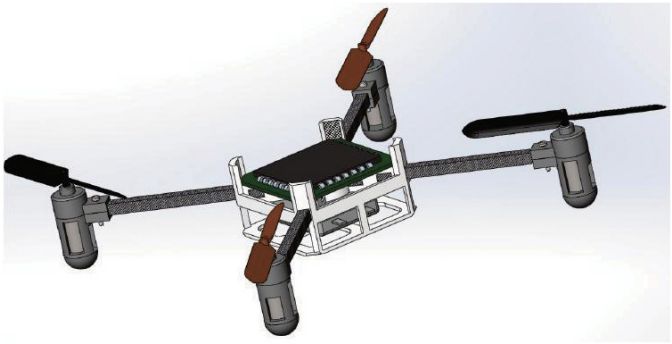

Fig. 9. Full micro quadrotor body designed in SolidWorks with dimension (in mm).

3.2. *Motor and propeller*

Motor and propeller sets are the main actuators of the quadrotor MAV. As each quadrotor consists of four sets of motor and propeller, they need to be chosen carefully as their characteristics must satisfy the design requirements. A few important design requirements of the quadrotor MAV, which are directly related to the characteristics of the motor and propeller, are listed below:

(1) *Operating Voltage*: Different motor has different maximum input voltage, depends mainly on the size of the motor, and the torque produced by the motor. In general, smaller motor has lower operating voltage, where the torque produced by such motor is also relatively lower. In radio-controlled (RC) aircrafts, the motor operating voltage is commonly rated in the multiple of 3.7 V, same as the output voltage for a single cell Lithium-polymer (LiPo) battery. In the MAV design, since majority of the components can be powered by voltage as low as 3.3 V, a single cell powered motor will be ideal to the design.
(2) *Current Consumption*: As motors are the main power drains for the MAV, the current consumption of the motor directly affects the capacity of the battery needed for the MAV to fly in a specific amount of time.
(3) *Weight*: Four motors contribute four times its weight to the MAV system, and thus affect the overall weight of the system heavily.
(4) *Maximum Thrust Produced*: The maximum thrust of four rotors could produce must be at least greater than the overall weight of the MAV, for MAV to take-off. Ideally it must be at least 1.5 times the weight of the quadrotor to realize more aggressive maneuver.

Based on the requirements stated above, a 8000 kV single cell brushed DC motor is utilized. Combined with four propellers, two with clockwise and another two with anticlockwise spinning blades, the total weight of a single motor and propeller set is approximately 4 g. The propellers used are made of plastic, 56 mm in length. This propeller is readily available in the market, as it is also used in many hobby-range RC quadrotor such as Walkera QR Ladybird, Hubsan mini Quad, and TRAXXAS QR-1. Test bench experiment has proven that the combination could produce a maximum thrust of 16 g each, which combined is approximately 1.5 times larger than the proposed MAV at 40 g.

4. Avionic System Design

In order to control and navigate the micro quadrotor UAV, a full onboard system is essential in the UAV design and implementation. A typical avionic system consists of [33]:

(1) An onboard processor to collect data, implement control laws, drive actuators and communicate with ground stations;

(2) An IMU to measure the attitudes of the vehicles;
(3) A good communication system to provide communication link with ground stations; and
(4) Power supply system sufficient to power up the whole UAV for a respectable duration.

Conventionally, for a UAV with higher payload limit, the onboard components, such as microprocessor, IMU, radio receiver, and the servo controller, are usually chosen from the commercially available products [27,32]. However, in the micro quadrotor design, the placement of these components need to be further optimized to reduce weight. In this section, a single PCB design incorporating the microprocessor, IMU, and motor speed controllers is proposed. The overall system architecture for the PCB design is shown in Fig. 10.

4.1. *Microprocessor*

In avionics, processor is the crux of the entire system. Within this compact MAV design, the functions of the processor include: (1) collecting data from IMU sensor via serial port; (2) receiving command from the receiver in the form of pulse position modulation (PPM) signal; (3) decoding and analyzing data; (4) implementing flight control algorithms; (5) forwarding control signals in the form of pulse width modulation (PWM) signal to ESC; and (6) sending logged data to the logger via the serial port.

In order to perform the above tasks, ATmega328P (see Fig. 11), a high performance Atmel 8-bit AVR RISC-based microcontroller is selected due to the presence of the following characteristics: (1) availability of various ports, such as UART, SPI and PWM ports; (2) low power consumption; and (3) programming convenience. Key parameters of ATmega328P are listed in Table 7 while the time taken to accomplish the tasks stated above is shown in Fig. 12. Multiple tests were conducted to ensure ATmega328P

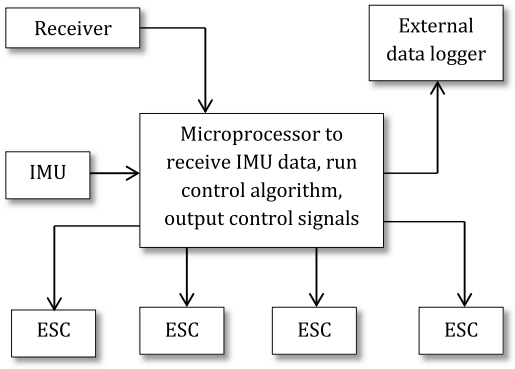

Fig. 10. Overall design architecture for micro quadrotor UAV onboard PCB design.

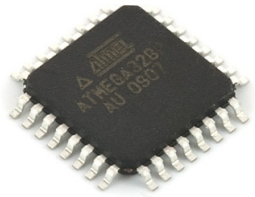

Fig. 11. ATmega328P,

microcontroller is capable of running the software and perform the tasks above within 5 ms. Thus, the control loop running in the software is user-configurable up to 200 Hz, depending on the update frequency of the IMU sensor.

4.2. *Inertial measurement unit*

IMU is an indispensable sensor to all autonomous aerial vehicles. It is attached to the aircraft to provide vital

Table 7. Key parameters of ATmega328P.

Key parameters of ATmega328P	
Flash memory	32 Kbytes
Pin count	32
Max. operating frequency	20 MHz
CPU	8-bit AVR
SPI	2
I2C	1
UART	1
PWM	6
ADC channels	8
Operating voltage	1.8–5.5 V
Active current consumption (1 MHz, 1.8 V)	0.2 mA

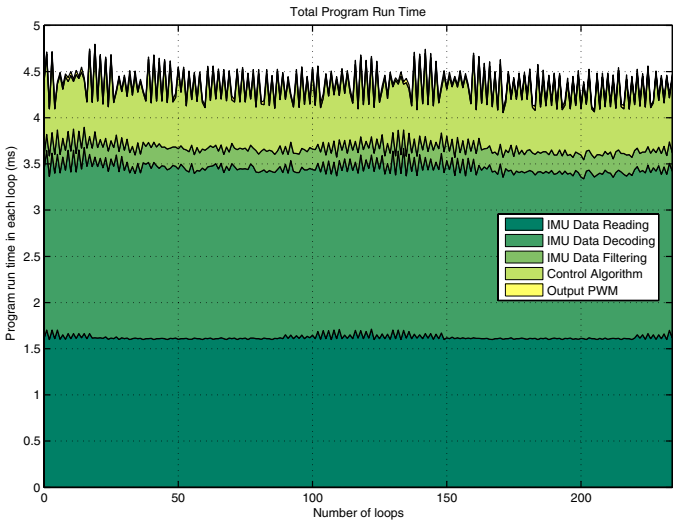

Fig. 12. Total program run time.

Fig. 13. VN-100 SMD.

real-time motion data such as accelerations, angular rates, and magnetic values. In addition, 3-axis Euler angles measurements are necessary for aircraft orientation control. However, IMU does not necessarily need to provide angular measurement of the aircraft as it can be estimated using an extended Kalman filter (EKF) [15] or complimentary filtering. The primary disadvantage of these filters is — they are computationally intensive, which add extra burden on the onboard AVR microprocessor. One of the solutions is to select a small, light yet powerful IMU with in-built EKF algorithm.

The VN-100 SMD (Fig. 13) from VectorNAV is selected as the onboard IMU. It is light weight (3 g) and miniature ($24 \times 22 \times 3$ mm) high performance IMU with Attitude Heading Reference System (AHRS). It is also built-in with 3-axis accelerometers, 3-axis gyros, 3-axis magnetic sensors as well as a 32-bit processor to compute and output a real-time plus drift-free 3D orientation solution.

Apart from that, VN-100 SMD chip also comprises a quaternion-based drift compensated Kalman filter operating with full 32-bit floating point precision by utilizing the on board 32-bit processor, which updates at 300 Hz according to the data provided. It also provides both raw and corrected sensor measurements as well as the estimated angles at 200 Hz.

Important specifications of VN-100 SMD chip is shown in Table 8.

Table 8. Important specifications of VN-100 SMD.

Specification of VN-100	
Yaw/Roll range	$\pm 180^\circ$
Pitch range	$\pm 90^\circ$
Angular rate range	$\pm 500^\circ$/s
Acceleration range	± 8 g
Power supply	3.2–5.5 V
Current drawn	50 mA @ 3.3 V
Communication	UART, SPI
Dimension	$24 \times 22 \times 3$ mm
Weight	3 g
Output data	Raw IMU data, Filtered Euler angles
Highest output data rate	200 Hz

Fig. 14. ATtiny13A.

4.3. *Brushed electronic speed controller*

ESC is the fundamental component for each brushed motor used in rotorcraft's design. The purpose of ESC is to convert PWM signal to analog signal, the waveform accepted as the input of the motor. MOSFET is used to boost the current of the analog signal such that it drives the motor directly from the power supply. In this ESC design, four 8 pins processors ATtiny13A (Fig. 14) are utilized as individual ESC to the motors. Four MOSFET chips are incorporated in the PCB as well.

4.4. *Radio-frequency receiver*

Typically in RC flights, a radio-frequency (RF) receiver is used to receive and decode RF signals sent from a transmitter controlled by a ground pilot. Receiver is not a requisite in a fully autonomous flight control system as no remote pilot is required. However, most of the UAV designs today retain the receiver component for failsafe purposes, where the ground pilot has higher authority to remotely control the UAV during emergencies, for example controller failures.

In this quadrotor MAV design, the receiver is implemented for a different objective. Apart from being able to receive control signal from a remote pilot, the receiver is used to receive control signals from a ground station in autonomous mode. It is effective especially operating in indoor environment with the aid of Vicon motion technology where the system measures the position and velocity of the MAV. Next, the Vicon system will transmit the control signals or the measurement values to the aircrafts onboard CPU via the transmitter-receiver link.

This communication link can be realized using PCTx cable, a product by Endurance R/C. The PCTx cable connects the ground station (desktop or laptop) to the transmitter which transmits the RF signal wirelessly to the onboard receiver. PPM signal is sent to the onboard CPU for processing upon receiving the signals from the ground station. The Rx31d manufactured by DelTang is selected for system integration due to its ultra tiny package of 10×10 mm with 0.21 g (see Fig. 15). It is capable of providing up to seven channels of PPM signals.

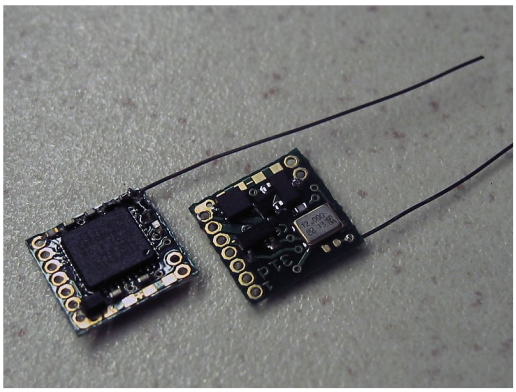

Fig. 15. DelTang Rx31d receiver.

Fig. 17. Power supply for the MAV.

4.5. *Data logger*

Important flight data such as state variables of an UAV are recorded for post flight observation and analysis, thus requiring a data logger. In order to fit into this MAV design, the data logger needs to be small, light and reliable to carry out this task. An open source data logger from Sparkfun OpenLog (see Fig. 16) is utilized for this purpose. OpenLog weighs only 1.70 g and fits perfectly into the MAV design. It starts logging any serial data up to 115,200 baud rate to the micro SD card upon powered up. In addition, Sparkfun provides OpenLog firmware and design files which can be redesigned into the main PCB of the MAV.

4.6. *Power supply*

The main consideration in designing the power supply is to meet the overall system and flight duration requirements. The choice of power supply is important as it usually constitutes approximately 30% of the overall weight of the MAV, and the power needed to lift the MAV will be increased due to its own weight. As all onboard components can be powered up with 3.3 V, a single cell LiPo battery with current capacity of 360 mAh is utilized to power the avionics and to drive the motors (see Fig. 17). A 3.3 V regulator is included to provide a clean voltage to the components, as a single cell LiPo battery has output vary from 4.2 V when fully charged to lower than 3.4 V when it is used up. The battery is as light as 10 g and is able to provide enough energy for an 8-min flight duration.

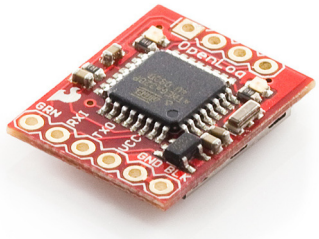

Fig. 16. Sparkfun OpenLog.

4.7. *PCB layout design*

In this subsection, the design process of the PCB for the avionic system of the micro quadrotor UAV will be described in detail. Among the five components to be included to the avionic system, the IMU, flight control CPU and four ESCs will be incorporated into the design, while the receiver and the logger will be attached to the designed PCB. A general guideline to design avionics PCB for quadrotor MAV using Altium Designer is as follows:

(1) *Schematic design* — A schematic diagram of the design must be drawn in Altium Designer with all the components needed, i.e., one ATmega328P, one VN-100 SMD, four ATtiny13As, and four MOSFETs. Also, four status indication LEDs are introduced to the design, with one of them connected directly to the power supply as the power indicator, while the rest of them connected to the general output port of the flight control CPU for user configurable purposes. As all these components can be powered up with 3.3 V, a voltage regulator with 3.3 V output is included. Connections between each of the components can be viewed in the schematics of ESC (see Fig. 18) and the microprocessor (see Fig. 19).

(2) *Layout assignment* — The layout of the components on the PCB is important as to reduce the electromagnetic interference between the components. To satisfy the dimension and weight constraints, a maximum of 4×4 cm PCB layout is imposed. The first component to

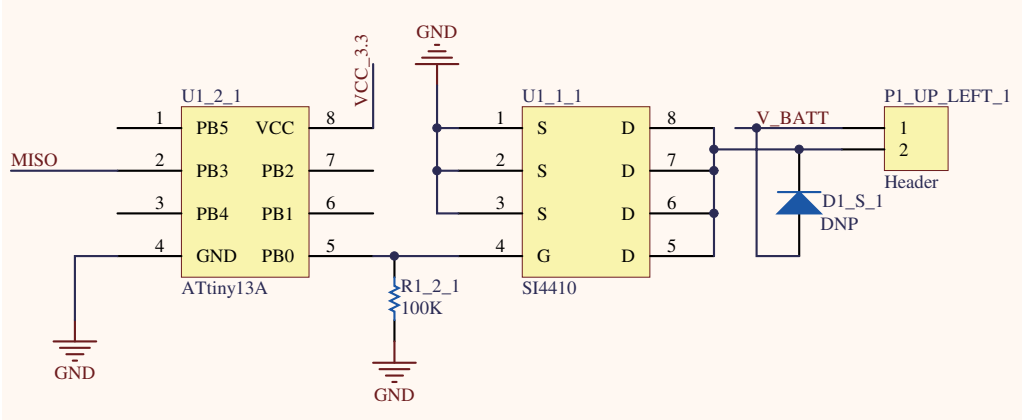

Fig. 18. Schematics of ESC.

be placed on the PCB is VN-100 SMD, as it must be placed in the middle of the design to be as close to the CG as possible. Its orientation is also an important issue to care of, as the *x*-axis of the component must be pointed to the front. Next, the flight control CPU, ATmega328P is placed in the middle of the opposite side of the PCB, while the four ESCs (one ATtiny13A and one MOSFET each) are placed at the four corner of the same side. Lastly, the four LEDs are placed beside the VN-100 SMD so that they are clearly visible to the user during flight.

(3) *Routing* — The final step of designing PCB is the routing to connect each component according to the connection assigned in the schematic phase. Note that the default distance measurement in Altium Designer is in unit mil (one-thousandth of an inch). The nonmain power routing is set to have a width of 10 mil, while the main power routing (3.7 V directly from power supply) is set to be 30 mil width to allow higher flow of current. The routing could be easily done (see Fig. 20) in a 2-layer-PCB setup.

Once the design is done, it can be sent to PCB manufacturer to fabricate. With PCB thickness of 1 mm, the fabricated product is approximately 7 g including all components, within the dimension of 40 × 40 × 1 mm. Table 9 details the total parts in the design of the micro quadrotor UAV, with specific weight budget assigned to each of them, together with the real weight of the manufactured components.

5. Mathematical Modeling of Micro Quadrotor UAV

To further understand the quadrotor system, a mathematical model of the system has to be derived. In literature, researchers from University of Pennsylvania have proven that a quadrotor system is a differential flat system, where

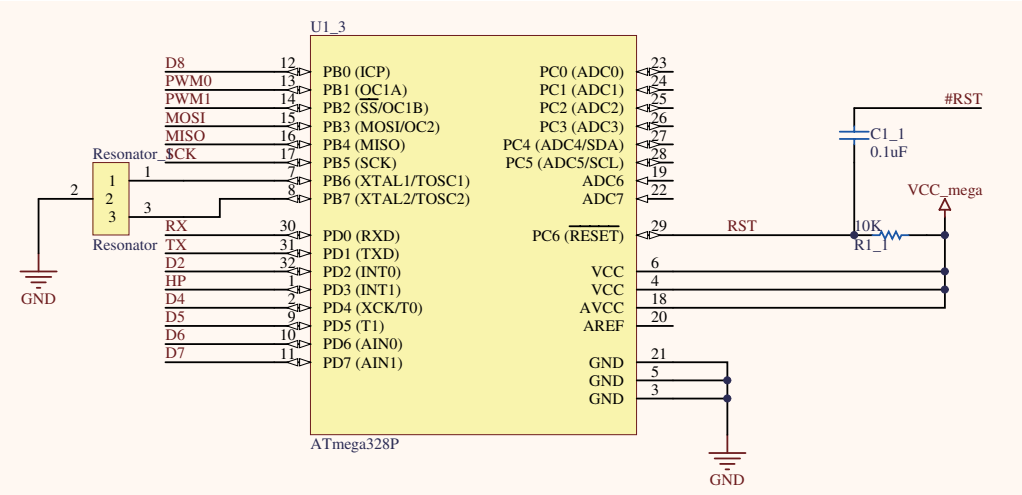

Fig. 19. Schematics of processor.

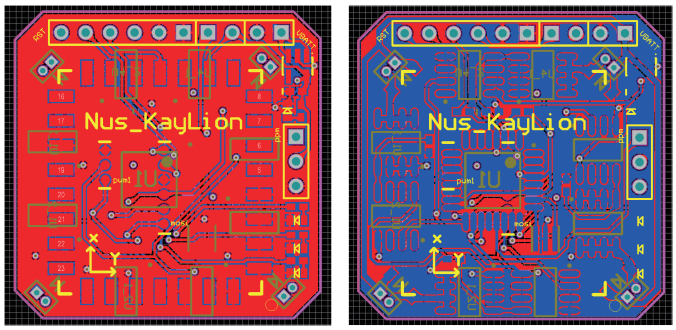

Fig. 20. PCB layout.

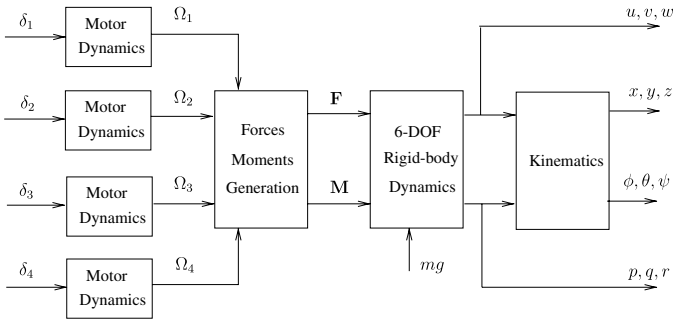

Fig. 21. Overview block diagram of the micro quadrotor UAV model.

the states and the inputs can be written as algebraic functions of four carefully selected flat outputs and their derivatives [22]. With this definition, the quadrotor model can be approximated as a double integrators linear system. However, in order to study the behavior of the quadrotor in aggressive maneuvering, a nonlinear quadrotor model will be needed.

Nonlinear quadrotor UAV model has been developed and revised by many researchers in the last decade [4, 29]. A major difference between the derived models from different researchers is the assignment of initial frame and body frame. Regarding frame assignments, this project follows a standard assignment of ground frame and body frame adopted by NUS UAV Research Group [5].

In this convention, the ground frame, also called North-East-Down (NED) frame, has its x-axis pointed to North, y-axis to East, and z-axis pointing downward into the ground. The origin of NED frame is fixed relative to the ground, at where the UAV powered up. As for the body frame, the origin of the frame will be located at the CG of the UAV, with x-axis pointing forward, y-axis pointing to the right, and z-axis pointing downwards of the UAV. Note that this body frame is fixed on the aircraft fuselage and will rotate and translate along with it.

With this frame convention, the derivation of the nonlinear mathematical model of the micro quadrotor UAV will be shown in the next subsections.

Table 9. Weight budget for micro quadrotor UAV.

Components	Amount	Estimate weight (g)	Current weight (g)
Battery	1	10	9.80
Motor and propeller	4	3.5	3.59
Quadrotor arm	4	1	0.93
Quadrotor frame	1	4	2.13
Avionic system	1	10	7.32
Miscellaneous		2	1.70
Total		44	39.03

5.1. *Overview*

The overview of the nonlinear model of micro quadrotor UAV is shown in Fig. 21. Inputs to the quadrotor, δ_n, shown on the left of the block diagrams, are the normalized PWM control signals sent from the microprocessor. Outputs of the model are the linear velocities u, v, w, linear positions x, y, z, Euler angles ϕ, θ, ψ, and angular velocities p, q, r shown on the right of the block diagram. Common symbols and variables to be used in the derivation are listed in the Nomenclature. Note that in the following derivation, the micro quadrotor has the cross configuration, with rotor numbers 1, 2, 3, 4 and basic working principle indicated in Fig. 22.

5.2. *Kinematics and rigid-body dynamics*

The translational and rotation motions between the NED and the body frame can be related with two well-known navigation equations [5]

$$\dot{\mathbf{P}}_{\mathbf{n}} = \mathbf{R}_{\mathbf{n/b}}\mathbf{V}_{\mathbf{b}}, \tag{1}$$

$$\dot{\Theta} = \mathbf{S}^{-1}\omega, \tag{2}$$

where the rotational matrix, $\mathbf{R}_{\mathbf{n/b}}$, and the lumped transformation matrix, $\mathbf{S}^{-1}$ are given by

$$\begin{aligned} \mathbf{R}_{\mathbf{n/b}} &= \begin{bmatrix} c_\theta c_\psi & s_\phi s_\theta c_\psi - c_\phi s_\psi & c_\phi s_\theta c_\psi + s_\phi s_\psi \\ c_\theta s_\psi & s_\phi s_\theta s_\psi + c_\phi c_\psi & c_\phi s_\theta s_\psi - s_\phi c_\psi \\ -s_\theta & s_\phi c_\theta & c_\phi c_\theta \end{bmatrix}, \\ \mathbf{S}^{-1} &= \begin{bmatrix} 1 & s_\phi t_\theta & c_\phi t_\theta \\ 0 & c_\phi & -s_\phi \\ 0 & s_\phi / c_\theta & c_\phi / c_\theta \end{bmatrix}, \end{aligned} \tag{3}$$

with $s_* = \sin(*)$, $c_* = \cos(*)$, and $t_* = \tan(*)$.

To describe the translational and rotational dynamics of any rigid-body, one can utilize the Newton–Euler

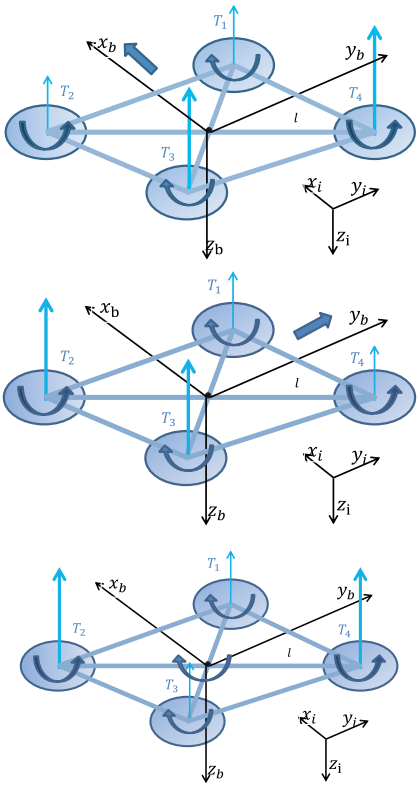

Fig. 22. Pitching, rolling and yawing for micro quadrotor UAV.

formalism as

$$m\dot{\mathbf{V}}_\mathbf{b} + \omega \times (m\mathbf{V}_\mathbf{b}) = \mathbf{F}, \tag{4}$$

$$\mathbf{J}\dot{\omega} + \omega \times (\mathbf{J}\omega) = \mathbf{M}, \tag{5}$$

where **F** and **M** are the force and moment vectors acting on the body. As the designed quadrotor is four way symmetrical, the inertia matrix of the micro quadrotor, **J**, is assumed to be diagonal, i.e.,

$$\mathbf{J} = \begin{bmatrix} J_{XX} & 0 & 0 \\ 0 & J_{YY} & 0 \\ 0 & 0 & J_{ZZ} \end{bmatrix}. \tag{6}$$

5.3. *Forces and moments generation*

Forces and moments generated by the aircraft contributed to its movement. They are generally generated by four different sources, i.e., the gravitational force, the rotors thrust and moment, its reaction torques, and the gyroscopic effects [3, 12]. Although the latter two have little significance on the overall forces and moments, they are included to provide a more complete model.

5.3.1. *Gravitational force and rotor movements*

Gravitational force and rotor movements contributed most of the overall forces and torques of the UAV. As the gravitational force acts only on the z-axis of the NED frame, by transforming it to the body frame, we have

$$\mathbf{F}_{\text{gravity}} = \mathbf{R}^{-1}_{\mathbf{n}/\mathbf{b}} \begin{bmatrix} 0 \\ 0 \\ mg \end{bmatrix} = \begin{bmatrix} -mgs_\theta \\ mgc_\theta s_\phi \\ mgc_\theta c_\phi \end{bmatrix}. \tag{7}$$

On the other hand, each of the rotating rotor creates a thrust, T_n, and a torque, Q_n, for $n = 1, 2, 3, 4$ along its axis. From the aerodynamics consideration, the thrust and torques produced can be modeled as

$$T_n = C_T \rho A r^2 \Omega_n^2, \tag{8}$$

$$Q_n = C_Q \rho A r^3 \Omega_n^2, \tag{9}$$

where C_T and C_Q are the aerodynamic coefficients of the propeller, ρ is the density of the air, A and r are the disc area swept by the rotating rotor and the radius of the rotor blade. Here, if we assume that the aerodynamic coefficients is a constant, which is generally the case when the collective pitch angle of the blade is fixed, the force and torque equations can be simplified to

$$T_n = k_T \Omega_n^2, \tag{10}$$

$$Q_n = k_Q \Omega_n^2, \tag{11}$$

where k_T and k_Q can be obtained easily through some experiments. With this simplification, the total thrusts of the micro quadrotor can be formulated as the summation of four individual thrust of the motors, i.e.,

$$\mathbf{F}_{\text{rotor}} = \begin{bmatrix} 0 \\ 0 \\ -(T_1 + T_2 + T_3 + T_4) \end{bmatrix}. \tag{12}$$

Note that the thrusts are pointing upwards, which is in the negative z-direction in our coordinate system. Next, pitch and roll moments will be generated by the thrust difference of the opposing rotors, with roll moment is contributed by thrust difference between rotor 2-3 and rotor 1-4 at x-axis, and pitch moment between rotor 1-2 and rotor 3-4 at y-axis. Lastly, yaw moment is generated based on the total moment of each rotors at z-axis. The moment vector will then be

$$\mathbf{M}_{\text{rotor}} = \begin{bmatrix} \frac{\sqrt{2}}{2} l(T_2 + T_3 - T_1 - T_4) \\ \frac{\sqrt{2}}{2} l(T_1 + T_2 - T_3 - T_4) \\ Q_1 + Q_3 - Q_2 - Q_4 \end{bmatrix}. \tag{13}$$

5.3.2. *Reaction torques*

Inertia counter torque, which is the reaction torque produced by the change in rotational speed of the rotor, is modeled as

$$\mathbf{M}_{\text{reaction}} = \begin{bmatrix} 0 \\ 0 \\ -J_r(\dot{\mathbf{\Omega}}_1 + \dot{\mathbf{\Omega}}_3 - \dot{\mathbf{\Omega}}_2 - \dot{\mathbf{\Omega}}_4) \end{bmatrix}. \tag{14}$$

5.3.3. *Gyroscopic effects*

Gyroscopic moments, caused by the combination of rotations of four propellers and the aircraft's body are commonly modeled as

$$\mathbf{M}_{\text{gyro}} = \sum_{i=1}^{4} J_r \left(\omega \times \begin{bmatrix} 0 \\ 0 \\ 1 \end{bmatrix} \right) (-1)^i \Omega_i \tag{15}$$

$$= \begin{bmatrix} -J_r q(\Omega_1 - \Omega_2 + \Omega_3 - \Omega_4) \\ J_r p(\Omega_1 - \Omega_2 + \Omega_3 - \Omega_4) \\ 0 \end{bmatrix}, \tag{16}$$

where J_r is the total rotational moment of inertia around the propeller axis.

5.4. *Motor dynamics*

A standard DC motor is usually a 2nd-order system, with one order contributed by the electrical dynamics, and another contributed by the mechanical dynamics. In most of the DC motor system, the electrical dynamics is much faster than the mechanical counterpart, and therefore we can approximate the motor dynamics as a first-order system, where its parameters, i.e., the steady state gain, k_m, and time constant, τ_m can be obtained experimentally. In frequency domain,

$$\frac{\Omega_n(s)}{\delta_n(s)} = \frac{k_m}{\tau_m s + 1}, \tag{17}$$

and in time domain,

$$\dot{\mathbf{\Omega}}_n = \frac{1}{\tau_m}[k_m(\delta_n - \delta_n^*) - \Omega_n], \tag{18}$$

where δ_n^* is the normalized input value right when the motor starts spinning. Note that in Eqs. (17) and (18), δ_n is the normalized input to the motor speed controller, with the following normalization process,

$$\delta_n = \frac{u_n - 1100}{840}, \tag{19}$$

where u_n is the PWM pulse width fed to the ESC in unit μs. In general, the minimum and maximum possible pulse widths to the ESC are at 1100 μs and 1940 μs, respectively.

5.5. *Parameters identification and verification*

Based on the model derived in the previous subsections, several parameters are to be identified with methods of direct measurement, software approximation and test bench experiments. Table 10 shows the parameters to be identified and its physical meaning.

5.5.1. *Direct measurements*

Some parameters can be directly measured by a weighing balance and ruler, as follows:

$$m = 0.045\,\text{kg}, \tag{20}$$

$$l = 0.058\,\text{m}, \tag{21}$$

where m is the gross weight and l is the beam length. The gravitational acceleration can be calculated given the latitude of Singapore as follows,

$$g \approx 9.781\,\text{m/s}^2. \tag{22}$$

5.5.2. *Software approximations*

With the aid of SolidWorks, the tensor and rotating moment of inertia of mechanical parts can be estimated numerically. With exact density and scale to the real physical parts, the tensor moment of inertia of the quadrotor MAV and the rotating moment of inertia of the propeller are calculated with the mass properties function of SolidWorks:

$$J = \begin{bmatrix} 3.0738 & 0 & 0 \\ 0 & 3.0849 & 0 \\ 0 & 0 & 5.9680 \end{bmatrix} \times 10^{-5}\,\text{kgm}^2, \tag{23}$$

Table 10. Parameters to be identified and its physical meaning.

Parameter	Physical meaning
g	Gravity acceleration
m	Mass of quadrotor
l	Distance between rotor and center of gravity
k_T	Rotor thrust constant
k_Q	Rotor torque constant
k_m	Motor steady-state gain
τ_m	Motor time constant
J_{XX}	Moment of inertia of quadrotor along x-axis
J_{YY}	Moment of inertia of quadrotor along y-axis
J_{ZZ}	Moment of inertia of quadrotor along z-axis
J_r	Rotating moment of inertia of propeller

$$J_r = 5.897 \times 10^{-8}\,\mathrm{kgm}^2. \quad (24)$$

Note that J is diagonal as the designed quadrotor structure is highly symmetric.

5.5.3. *Test bench experiments*

Some aerodynamic parameters need to be measured and calculated by bench experiment instead of direct measurement. These parameters include the thrust coefficient, torque coefficient, as well as the motor dynamic parameters. A lever-balance setup is realized to measure the thrust coefficient of the rotor. A customized miniature infrared RPM reader is used to measure the time interval between two adjacent cutting of the propeller, where the real-time angular velocities can be calculated. With the values read from the weighing scale for a few different input voltage to the motor, the corresponding thrust produced is obtained and plotted against its angular speed square, as shown in Fig. 23. Thrust coefficient k_T can then be approximated as the gradient of the trend line. Similarly, the torque coefficient of the rotor can also be measured by a similar setup. Figure 24 illustrates the relationship between the rotational speed of the motor and the torque produced. The thrust and the torque coefficients are obtained as follows:

$$k_T = 3.334 \times 10^{-8}\,\mathrm{N}/(\mathrm{rad}^2/\mathrm{s}^2), \quad (25)$$

$$k_Q = 1.058 \times 10^{-10}\,\mathrm{Nm}/(\mathrm{rad}^2/\mathrm{s}^2). \quad (26)$$

Parameter identification of brushed motor dynamics is also conducted with the similar setup. Constant input of several different values is fed to the motor, and the resultant angular speeds of the rotor are recorded. In Fig. 25, the asterisk data points show the experiment results of angular speed against input value and the straight line shows the trend based on the assumption that the motor steady state velocity is proportional to the input value at the motor operating point (while the UAV is at hover condition). Thus, the steady state gain k_m can be extracted. As the transient property of the motor can be described as a first-order process, the average time constant τ_m is estimated from the transient response of a step input to the motor. They are

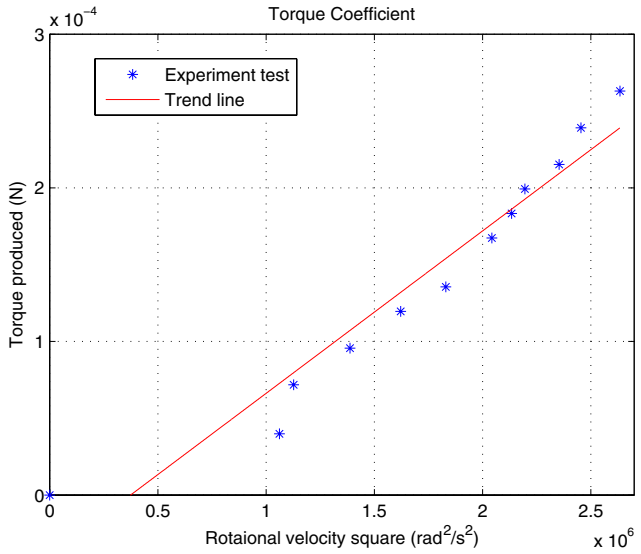

Fig. 24. Torque against square of motor rotational speed.

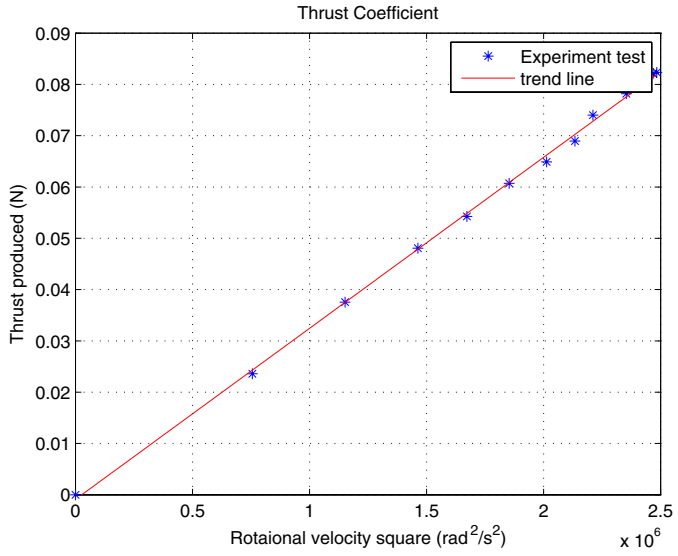

Fig. 23. Thrust against square of motor rotational speed.

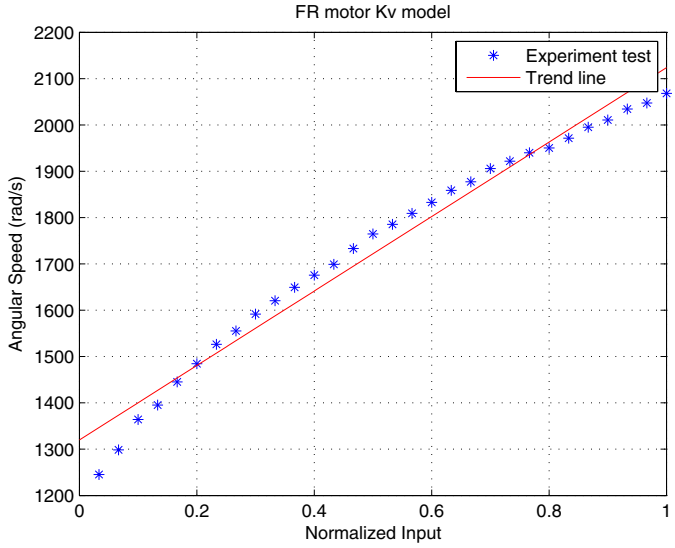

Fig. 25. Motor's angular speed against normalized PWM input.

Table 11. Parameters identified.

Parameters	Values
m	0.045 kg
g	9.781 m/s^2
l	0.058 m
k_T	3.334×10^{-8} N/(rad^2/s^2)
k_Q	1.058×10^{-10} Nm/(rad^2/s^2)
k_m	803.9
τ_m	0.0821 s
J_{XX}	3.0738×10^{-5} kgm^2
J_{YY}	3.0849×10^{-5} kgm^2
J_{ZZ}	5.9680×10^{-5} kgm^2
J_r	5.897×10^{-8} kgm^2

identified as follows:

$$k_m = 803.9, \tag{27}$$

$$\tau_m = 0.0821\,\text{s}. \tag{28}$$

Table 11 summarizes the parameters identified in the above sections.

6. MAV Control

Upon obtaining the mathematical model of the aircraft, a simple yet reliable PID controller is designed and simulated with the aid of Simulink in MATLAB.

Generally, the dynamics of a quadrotor without orientation stabilizer is too fast even for a skilled man pilot. The fast dynamic is contributed by the roll and pitch movements, while the yaw movement exhibits a much slower dynamic.

In this section, an orientation controller is described and implemented to achieve attitude stability of the micro quadrotor UAV. The controller is first designed in Simulink and MATLAB onto the mathematical system derived and estimated in the previous section. Upon obtaining a satisfying control response in simulation, the controller is then realized in the micro quadrotor hardware. The mathematical model is then verified with sinusoidal perturbation inputs.

6.1. *Software simulation*

In the initial stage of the PID gains tuning, the controller is first designed in simulation by adopting the Ziegler–Nichols method, as shown in the steps below:

(1) Set both derivative (K_d) and integrative (K_i) gain to zero, tune proportional gain (K_p) such that simulation results shows sustained oscillation on all Euler angles.

Table 12. Zielger–Nichols PID tuning method.

	K_p	K_i	K_d
classic PID	$0.6K_u$	$2K_p/T_u$	$K_pT_u/8$

(2) Record the ultimate proportional gain (K_u) and the oscillation period (T_u).
(3) Adjust PID gains based on classical Zeigler–Nichols PID tuning method, as shown in Table 12.

Simulated result in Fig. 26 has shown a stable quadrotor system, with all the Euler angles and angular rates signals are attenuated to zero within 5 s. This set of PID gains will later be used as an initial values to apply to the real quadrotor system. It should be noted that the simulation is carried out at the theoretical trim values of the PWM inputs, which is at 1500 μs.

6.2. *Hardware realization*

Once a reasonable simulation result is obtained, the PID controllers are realized in the MAV hardware. The controllers on yaw, pitch and roll angles are first tested separately on a single axis setup, where the quadrotor MAV is able to rotate at only one axis, for example, the y-axis (pitch). The same PID controller designed in the simulation was implemented to the system, followed by further fine-tuning of the gains, axis by axis. After the tuning process, a set of PID gains for each axis in which the aircraft is able to stabilize horizontally on this setup was obtained, as shown in Table 13.

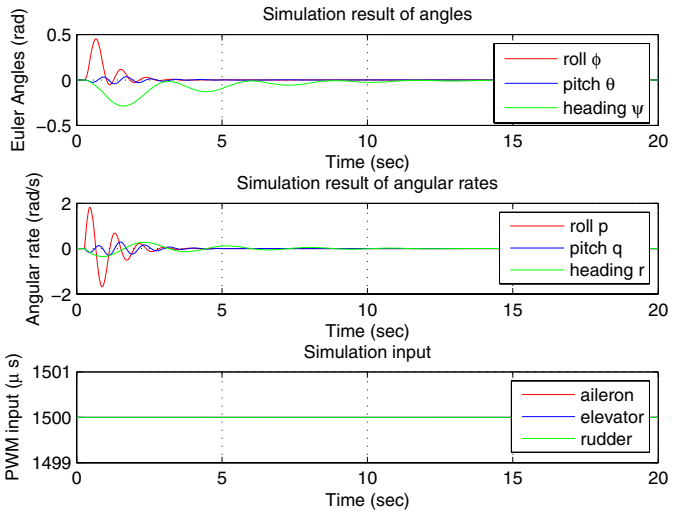

Fig. 26. Simulation results with PID gains.

Table 13. PID gains implemented to the quadrotor MAV.

Channel	K_p	K_i	K_d
Pitch	1.60	2.45	0.51
Roll	1.60	2.45	0.51
Yaw	4.00	0.75	0.10

Next, the PID controller is realized in the manufactured quadrotor MAV codenamed KayLion (Fig. 27). Flight tests are carried out to test the endurance of the vehicle, and to verify the mathematical model derived in the previous section.

In particular, chirp-like oscillating inputs are sent to the MAV system, while its Euler angles and angular rates responses are recorded in the onboard logger. A chirp-like input is an oscillating signal sent to the quadrotor with varied frequency. The angular response of the quadrotor corresponds to this frequency band is recorded to build a complete frequency response of the system. It is then compared to the simulated responses by using the exact inputs to the simulator. Figure 28 shows the perturbation signal on elevator channel to the MAV, while Fig. 29 shows the responses of the system in pitch direction plotted together with the simulated results. Besides some random low amplitude oscillations caused by the disturbances from the air movement, the responses match fairly well. The roll response is assumed to be similar to the pitch response, as the quadrotor MAV is four way symmetrical.

In the other flight test, a chirp-like signal was injected to the throttle channel of the quadrotor MAV, resulting in agitated heave movement. In this experiment, a Vicon motion tracking system is used to measure the position of the quadrotor with reference to the start up origin. A more detailed description of this Vicon system will be shown in the next subsection.

With the measured z-position, the corresponding velocity respond will be computed. Both the input signals and computed z-axis velocity are logged and plotted in Figs. 30 and 31. In the latter figure, it can be seen that the derived mathematical model on heave movement matches well with the experimental data to a certain perturbation frequency, which is approximately 1 Hz. The quadrotor MAV was

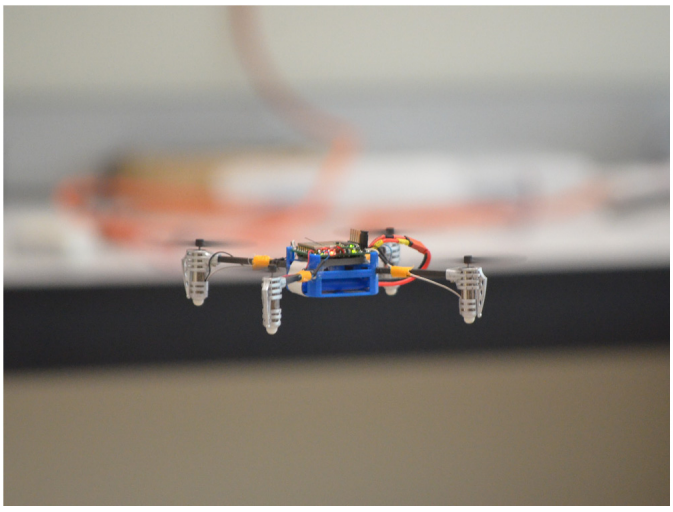

Fig. 27. A full working prototype quadrotor MAV, KayLion, designed and built by the National University of Singapore (NUS).

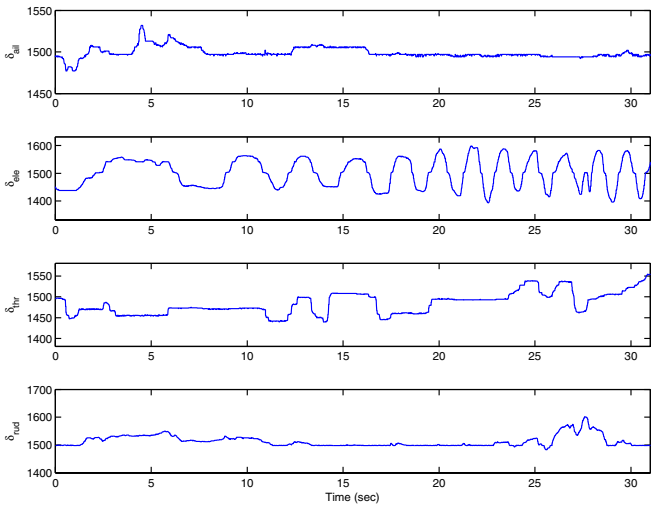

Fig. 28. Input to the MAV system in pitch perturbation test.

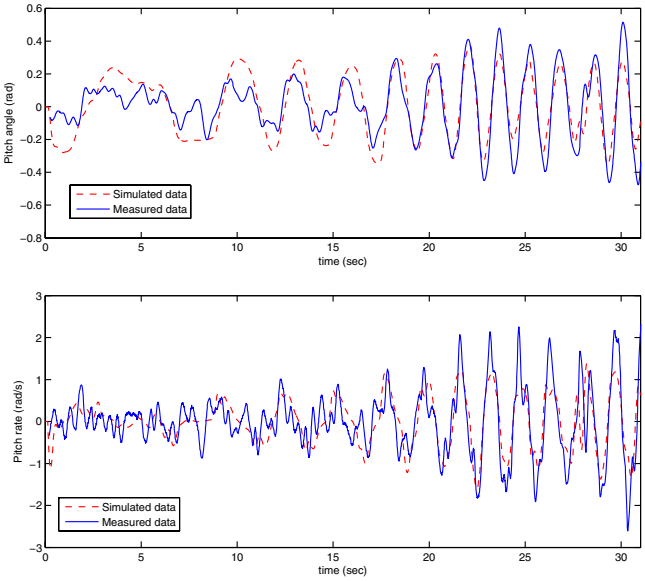

Fig. 29. Pitch angle and angular rate of the system response together with simulated response.

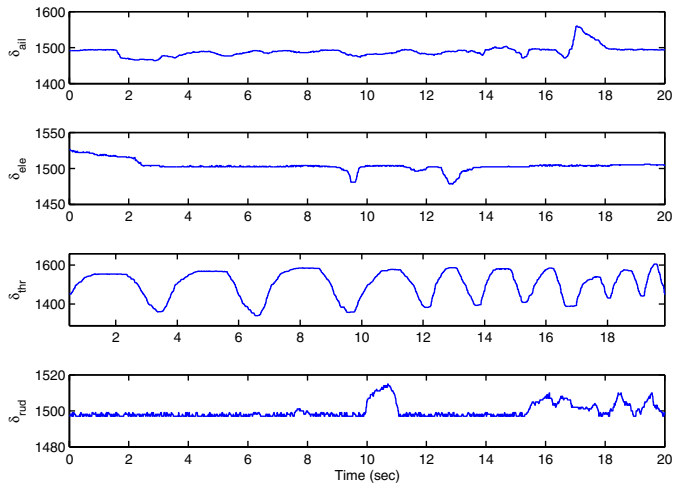

Fig. 30. Input to the MAV system in heave perturbation test.

unable to respond to the perturbation signal above this frequency, as it can be observed with naked eyes during the flight tests.

6.3. *Full six degree of freedoms autonomous control*

A full autonomous MAV control, including three-degree orientation control and three-degree translational control, is realized in the presence of Vicon motion tracking system. In this system, several infrared cameras are installed around the flyable area of the closed room, where they are used to detect reflective markers mounted on the aircraft fuselage. The system then estimate the orientation and position of the aircraft, based on the estimated positions of the reflective markers. In the NUS Vicon setup, 10 cameras are used to provide up to 0.1 mm accuracy of the estimated

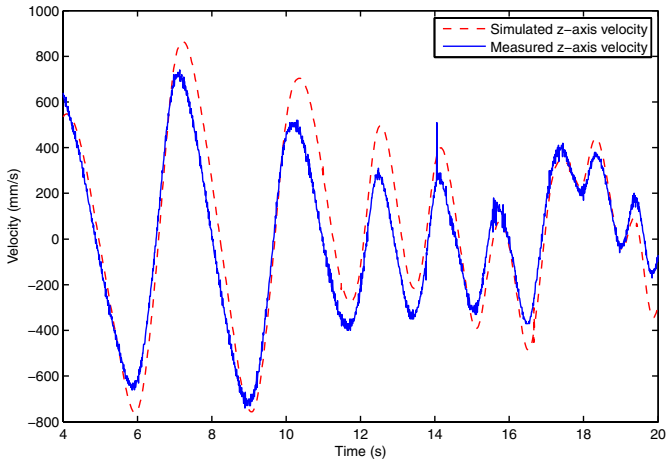

Fig. 31. Heave velocity response of the UAV together with simulated response.

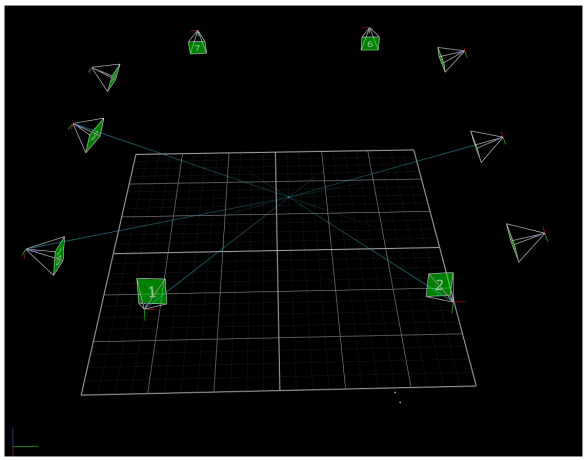

Fig. 32. Position of 10 cameras in the Vicon system.

position of the markers. The position information is then sent up to the quadrotor MAV for further processing to realize position control and trajectory tracking. Figure 32 shows the 6×6 m coverage area in the Vicon motion tracking system in NUS.

The quadrotor is commanded to track a square path with 3.6 m side length. The orientation of the quadrotor was stabilized with a linear quadratic regulator (LQR) controller, while the position control of the MAV is realized in PID control structure. The position response of the autonomous system is shown in Fig. 33. The MAV is able to track the *x*- and *y*-positions fairly well, while remains ± 3 cm error on the *z*-position. This difference is due to the dynamics of the difference channel, as the *x*- and *y*-channels dynamics are much higher than the *z*-channel's, and thus more prone to surrounding noise.

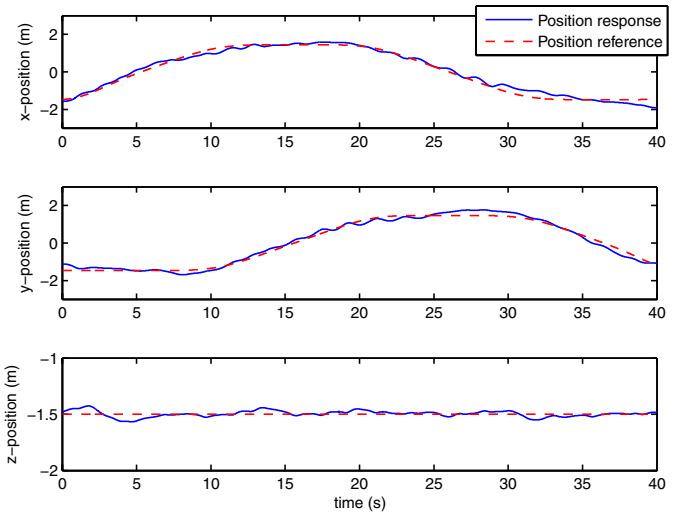

Fig. 33. Position reference and response of the quadrotor in full autonomous flight test.

7. Conclusion and Future Works

This paper has shown a general guideline to systematically design a micro quadrotor UAV, which has a gross weight of about 40 g. The design procedure is divided into three major sections. First, FEA is carried out to obtain a suitable dimension and shape of the carbon fiber beams as the main structure of the UAV. A sectional conclusion was made based on the analysis results and the weight constrain on the quadrotor body, that the square (or round) hollow beam of carbon fiber is the most weight optimum shape for quadrotor arms design. It appears to be the stiffest among other shape candidates of similar weight category.

Next, the avionic system of the micro quadrotor UAV is discussed in detail. An all-in-one PCB which include sensors, microprocessors and four ESCs is proposed and carefully designed in order to fit the application of our micro quadrotor UAV under the weight constraint. The designed system included a powerful light weight AHRS, VN-100 from VectorNAV, directly soldered on the board. The design is verified and debugged, then outsourced for fabricating. The whole avionic system is less than 8 g, which is a milestone where no other commercially available products could reach.

In the next section, a nonlinear mathematic model of the micro quadrotor is derived, based on Newton–Euler formalism. Method of identifying each parameters is also mentioned. This model has been verified to be quite accurately representing the quadrotor MAV. Autonomous flight tests video demonstration can be viewed on the NUS UAV YouTube channel, or http://youtube/uoPoGdOVWfs.

The micro quadrotor UAV will serve as a good platform to implement and realize control algorithms. Advanced model-based controller such as LQR and H-infinity controllers can be designed and implemented as the fairly accurate mathematical model and the micro quadrotor hardware are both readily available. A vision subsystem can also be included to the avionics of the MAV, to realize applications such as search and rescue, and indoor surveillance.

References

[1] M. Achtelik, A. Bachrach, R. He, S. Prentice and N. Roy, Autonomous navigation and exploration of a quadrotor helicopter in GPS-denied indoor environments, *IEEE Int. Conf. Robotics and Automation*, Kobe (2009).

[2] V. Arabagi, L. Hines and M. Sitti, Design and manufacturing of a controllable miniature flapping wing robotic platform, *Int. J. Robot. Res.* **31**(6) (2012) 785–800.

[3] S. Bouabdallah, P. Murrieri and R. Siegwart, Design and control of an indoor micro quadrotor, *IEEE Int. Conf. Robotics and Automation*, New Orleans, LA, USA (2004), pp. 4393–4398.

[4] T. Bresciani, Modelling, identification and control of a quadrotor helicopter, Master thesis, Lund University, Lund, Sweden (2008).

[5] G. Cai, B. M. Chen and T. H. Lee, *Unmanned Rotorcraft Systems* (Springer, London/New York, 2011).

[6] G. Cai, F. Lin, B. M. Chen and T. H. Lee, Systematic design methodology and construction of UAV helicopters, *Mechatronics* **18**(10) (2008) 545–558.

[7] E. Capello, A. Scola, G. Guglieri and F. Quagliotti, Mini quadrotor UAV: design and experiment, *J. Aerosp. Eng.* **25**(4) (2012) 559–573.

[8] A. Ceruti, A. Liverani and L. Recanatesi, Improving helicopter flight simulation with rotor vibrations, *Int. Conf. Innovative Methods in Product Design*, Venice, Italy (2011), pp. 636–645.

[9] J. Chao, Extractor X — autonomous tilt rotor UAV, *Unmanned Syst.*, **1**(2) (2013) 177–198.

[10] A. Di Cesare, K. Gustafson and P. Lindenfelzer, Design optimization of a quadrotor capable of autonomous flight, Final Year Thesis, Worchester Polytechnic Institute, Worcester, MA (2008).

[11] M. A. A. Fenelon and T. Furukawa, Design of an active flapping wing mechanism and a micro aerial vehicle using a rotary actuator, *Mech. Mach. Theory* **45**(2) (2010) 137–146.

[12] R. Goel, S. M. Shah, N. K. Gupta and N. Ananthkrishnan, Modeling, simulation and flight testing of an autonomous quadrotor, in *Proc. Int. Conf. Environmental and Agriculture Engineering*, Bangalore, India (2009).

[13] C. K. Hsu, J. Evans, S. Vytla and P. G. Huang, Development of flapping wing micro air vehicles-design, CFD, experiment and actual flight, in *Proc. 48th AIAA Aerospace Sciences Meeting Including the New Horizons Forum and Aerospace Exposition*, Orlando, FL, USA (2010).

[14] M. A. Hossain, F. Hasan, A. F. M. T. Seraz and S. A. Rajib, Development of design and manufacturing of a fixed wing radio controlled micro air vehicle, *MIST Journal: GALAXY (DHAKA)* **3** (2011).

[15] J. S. Jang and D. Liccardo, Small UAV automation using MEMS, *IEEE Aerosp. Electron. Syst. Mag.* **22** (2007) 30–34.

[16] K. Jackson, J. Li, E. Timmons and J. Wallace, icarusLabs: An adventure in crowdsourcing, *Unmanned Syst.* **1**(2) (2013) 199–209.

[17] K. Kang and J. V. R. Prasad, Development and flight test evaluations of an autonomous obstacle avoidance system for a rotary-wing UAV, *Unmanned Syst.* **1**(1) (2013) 3–19.

[18] M. Keennon, K. Klingebiel, H. Won and A. Andriukov, Development of the nano hummingbird: A tailless flapping wing micro air vehicle, *AIAA Aerospace Sciences Meeting*, Nashville, TN, USA (2012).

[19] F. Lin, K. Ang, F. Wang, B. M. Chen *et al.*, Development of an unmanned coaxial rotorcraft for the DARPA UAVForge challenge, *Unmanned Syst.*, **1**(2) (2013) 211–245.

[20] L. Meier, P. Tanskanen, F. Fraundorfer and M. Pollefeys, Pixhawk: A system for autonomous flight using onboard computer vision, *2011 IEEE Int. Conf. Robotics and Automation*, Shanghai, China (2011), pp. 2992–2997.

[21] D. Mellinger, M. Shomin and V. Kumar, Control of quadrotors for robust perching and landing, in *Proc. Int. Powered Lift Conf.* Philadelphia, PA, USA (2010), pp. 119–126.

[22] D. Mellinger and V. Kumar, Minimum snap trajectory generation and control for quadrotors, *2011 IEEE Int. Conf. Robotics and Automation (ICRA)*, Shanghai, China (2011), pp. 2520–2525.

[23] K. Nonami, F. Kendoul, S. Suzuki, W. Wang and D. Nakazawa, Development of autonomous quad-tilt-wing (QTW) unmanned aerial vehicle: Design, modeling, and control, in *Autonomous Flying Robots* (Springer, Japan, 2010), pp. 77–93.

[24] A. A. Paranjape, S. J. Chung, H. H. Hilton and A. Chakravarthy, Dynamics and performance of tailless micro aerial vehicle with flexible articulated wings, *AIAA J.* **50**(5) (2012) 1177–1188.

[25] G. de Pasquale and A. Soma, Reliability testing procedure for MEMS IMUs applied to vibrating environments, *Sensors* **10**(1) (2010) 456–474.

[26] J. M. Pflimlin, P. Binetti, P. Soueres, T. Hamel and D. Trouchet, Modeling and attitude control analysis of a ducted-fan micro aerial vehicle, *Control Eng. Pract.* **18**(3) (2010) 209–218.
[27] S. K. Phang, J. J. Ong, T. C. R. Yeo, B. M. Chen and T. H. Lee, Autonomous mini-UAV for indoor flight with embedded on-board vision processing as navigation system, in *Proc. IEEE R8 Int. Conf. Computational Technologies in Electrical and Electronics Engineering*, Irkutsk Listvyanka, Russia (2010), pp. 722–727.
[28] G. N. M. Plasencia, M. T. Rodriguez, S. C. Rivera and A. H. Lopez, Modelling and analysis of vibrations in a UAV helicopter with a vision system, *Int. J. Adv. Robot. Syst.* **9** (2012).
[29] G. V. Raffo, M. G. Ortega and F. R. Rubio, An integral predictive/nonlinear H∞ control structure for a quadrotor helicopter, *Automatica* **46** (2010) 29–39.
[30] J. Ratti, J. H. Moon and G. Vachtsevanos, Towards low-power, low-profile avionics architecture and control for micro aerial vehicles, *IEEE Aerospace Conf.*, Montana, US (2011), pp. 1–8.
[31] E. Ulrich, D. Pines and J. Humbert, From falling to flying: The path to powered flight of a robotic samara nano air vehicle, *Bioinspir. Biomim.* **5** (2010).
[32] F. Wang, S. K. Phang, J. Cui, B. M. Chen and T. H. Lee, Search and rescue: A UAV aiding approach, in *Proc. 23rd Canadian Congress of Applied Mechanics*, Vancouver, Canada (2011), pp. 183–186.
[33] F. Wang, S. K. Phang, J. J. Ong, B. M. Chen and T. H. Lee, Design and construction methodology of an indoor UAV system with embedded vision, *Control Intell. Syst.* **40**(1) (2012) 22–32.

Swee King Phang was born in Kuala Lumpur, Malaysia, in 1986. He received his B.Eng. degree with First Class Honors in the Department of Electrical and Computer Engineering at National University of Singapore (NUS) in 2010. He is currently a research scholar from NUS Graduate School for Integrative Sciences and Engineering (NGS) for his Ph.D. degree study. His research interests lie in the development of micro unmanned aerial vehicle (MAV), which include UAV construction, control theory application, and indoor navigation. He was the recipient of the IEEE Control Systems Chapter Book Prize, Singapore (2010). He is a student member of IEEE since 2009 and a student member of AIAA since 2010.

Kun Li received his Bachelor degree in Department of Control Science and Engineering from Zhejiang University, China. He is currently pursuing his Ph.D. degree in Department of Electrical and Computer Engineering from National University of Singapore, Singapore. His research interests include UAV Platform Design, Modeling and Control.

Kok Hwa Yu received his B.Sc. (Hons) and M.Sc. degrees in Aerospace Engineering from Universiti Sains Malaysia in 2008 and 2011. Presently, he is pursuing his doctorate in the Department of Mechanical Engineering in National University of Singapore.

Ben M. Chen received a B.S. degree in mathematics and computer science from Xiamen University, Xiamen, China, in 1983, an M.S. degree in electrical engineering from Gonzaga University, Spokane, Washington, USA, in 1988, and a Ph.D. degree in electrical & computer engineering from Washington State University, Pullman, Washington, USA, in 1991. He is currently a Professor in Department of Electrical and Computer Engineering, National University of Singapore. His current research interests are in systems and control, unmanned aerial systems, and financial market modeling. Dr. Chen is an IEEE Fellow. He is the author/co-author of nine research monographs including *Loop Transfer Recovery*: *Analysis and Design* (Springer, London, 1993), *H2 Optimal Control* (Prentice Hall, London, 1995), *Robust and H Control* (Springer, New York, 2000), *Hard Disk Drive Servo Systems* (Springer, New York, 1st Edition, 2002; 2nd Edition, 2006), *Linear Systems Theory*: *A Structural Decomposition Approach* (Birkhauser, Boston, 2004), *Unmanned Rotorcraft Systems* (Springer, New York, 2011), and *Stock Market Modeling and Forecasting*: *A System Adaptation Approach* (Springer, New York, 2013).

He currently serves as an editor-in-chief of *Unmanned Systems* and a deputy editor-in-chief of *Journal of Control Theory & Applications*. He had also served on the editorial boards of a number of journals including *IEEE Transactions on Automatic Control, Systems & Control Letters, and Automatica*. He was the recipient of Best Poster Paper Award, *2nd Asian Control Conference*, Seoul, Korea (1997); IES Prestigious Engineering Achievement Award, Institution of Engineers, Singapore (2001); Temasek Young Investigator Award, Defence Science & Technology Agency, Singapore (2003); Best Industrial Control Application Prize, *5th Asian Control Conference*, Melbourne, Australia (2004); Best Application Paper Award, *7th Asian Control Conference*, Hong Kong (2009), and Best Application Paper Award, *8th World Congress on Intelligent Control and Automation*, Jinan, China (2010). His unmanned systems team, GremLion, was selected as one of the nine finalists, out of 144 teams from 153 countries, to take part in the final fly-off in the 2012 DARPA UAVForge Challenge, held in Fort Stewart, Georgia, USA. The Challenge, with no winner declared, was jointly organized by the Defense Advanced Research Projects Agency (DARPA) and Space and Naval Warfare Systems Center Atlantic (SSC Atlantic), USA. His rotorcraft team was ranked the first in the final round of the Rotary-Wing Competition, and his unconventional aircraft team received a New Innovation Star Award in the 2013 AVIC Cup — International UAV Innovation Grand Prix, held in Beijing, China.

Tong Heng Lee received the B.A. degree with First Class Honours in the Engineering Tripos from Cambridge University, England, in 1980; the M.Eng. degree from NUS in 1985; and the Ph.D. degree from Yale University in 1987. He is a Professor in the Department of Electrical and Computer Engineering at the National University of Singapore (NUS); and also a Professor in the NUS Graduate School, NUS NGS. He was a past Vice-President (Research) of NUS.

Dr. Lee's research interests are in the areas of adaptive systems, knowledge-based control, intelligent mechatronics and computational intelligence. He currently holds Associate Editor appointments in the *IEEE Transactions in Systems*, *Man and Cybernetics*; *IEEE Transactions in Industrial Electronics*; *Control Engineering Practice* (an IFAC journal); and the *International Journal of Systems Science* (Taylor and Francis, London). In addition, he is the Deputy Editor-in-Chief of IFAC Mechatronics journal.

Dr. Lee was a recipient of the Cambridge University Charles Baker Prize in Engineering; the 2004 ASCC (Melbourne) Best Industrial Control Application Paper Prize; the 2009 IEEE ICMA Best Paper in Automation Prize; and the 2009 ASCC Best Application Paper Prize. He has also co-authored five research monographs (books), and holds four patents (two of which are in the technology area of adaptive systems, and the other two are in the area of intelligent mechatronics). He is the recipient of the 2013 ACA Wook Hyun Kwon Education Prize.